Motions of spiral waves in oscillatory media and in the presence of obstacles

J.A. Sepulchre* and A. Babloyantz
Service de Chimie-Physique, Université Libre de Bruxelles, Code Postal 231, Campus Plaine, Boulevard du Triomphe, B-1050 Bruxelles, Belgium
(Received 4 January 1993)

The properties of spiral-wave propagation in oscillatory and finite media are considered. Several different types of trajectories of the spiral core are seen, as the distance from the boundaries is increased. The size and the location of obstacles modify the motion of the spiral cores.

PACS number(s): 05.45.+b, 82.40.Ck, 02.60.Cb

I. INTRODUCTION

The behavior of spatial patterns in small systems is an important issue as several experimental setups are of rather small size. For example, Davidenko *et al.* study the onset of spiral waves *in vitro* in a small piece of heart tissue of size 20×20 mm^2 [1]. Another example is given by the study of intracellular propagation of calcium waves [2]. In small systems boundary effects may induce patterns which are not present in infinite systems.

In this paper we report the properties of spiral waves when they are created in a small oscillating system. By a small system we mean a system which has a size of the order of a few wavelengths. Our study is based on numerical simulations of generic model equations, such as the complex Ginzburg-Landau equation and also the Brusselator model, both in a nonturbulent regime.

The spiral is created by introducing a topological defect in the system. It is seen that zero-flux boundary conditions may constrain the defect, situated at the center of the spiral, to drift along the boundaries of the system. In general, the defect follows simple trajectories in a translational motion. In some cases the translational motion is accompanied with a rotational motion which gives rise to a *looping*-type trajectory. We focus on the dependence of these trajectories on the initial position of the defect, on the geometrical shape of the system, and on the relaxational character of the oscillations. An interesting point is that these trajectories may converge asymptotically to several closed circuits, which are attracting for nearby initial conditions. These circuits are followed by the defects in a strictly periodic way and thus reflect the existence of global-limit cycles of the dynamics.

Some phenomena are also reported when impermeable barriers (obstacles) are present in the system. These barriers may annihilate or create new defects in the medium.

In Sec. II a description of the models is given, together with some basic properties of spiral waves in oscillatory media. In Sec. III we report our numerical results for a system near the Hopf bifurcation. Trajectories in square and circular geometries are compared. Section IV is devoted to the same numerical experiments, but with relaxation oscillations. In Sec. V, we report results concerning propagation of spiral waves in the presence of obstacles. Section VI has a general discussion and conclusions.

II. SPIRAL WAVES IN OSCILLATORY MEDIA

This section is devoted to oscillatory media subject to dynamics which obey the complex Ginzburg-Landau equation (CGL). This equation describes the slow-amplitude modulation of the variables of a system close to a supercritical Hopf bifurcation [3, 4]. The CGL equation possesses a large range of applications, from the physics of lasers [5] to the study of cell aggregation in biology [6]. The CGL equation is given by

$$\frac{\partial W}{\partial t} = W - (1+i\beta)|W|^2 W + (1+i\alpha)\nabla_{\mathbf{x}}^2 W \ , \qquad (1)$$

where ∇^2 denotes the Laplacian operator in two-dimensional space and $W = U + iV$ is a complex variable. The boundary conditions are of the zero-flux type, i.e., the field W satisfies $\mathbf{n}\cdot\nabla W = 0$ on the boundaries, where $\mathbf{n}$ is the normal vector to the boundary of the system.

As in Sec. IV, relaxational oscillatory behavior will also be considered, using the well-known Brusselator model [7, 8], for the sake of uniformity of the exposition, we give the conditions under which the CGL equation is a good description of the Brusselator model. The equations of the model are

$$\begin{aligned} \frac{\partial X}{\partial \tau} &= A - (B+1)X + X^2 Y + D_X \nabla_{\mathbf{r}}^2 X \ , \\ \frac{\partial Y}{\partial \tau} &= BX - X^2 Y + D_Y \nabla_{\mathbf{r}}^2 Y \ . \end{aligned} \qquad (2)$$

In the Brusselator model, the unique stationary state $(A, B/A)$ loses its stability via a Hopf bifurcation when parameter $B > B_H = 1 + A^2$. The distance from the bifurcation point may be measured with the parameter ϵ defined as $\epsilon = \sqrt{(B - B_H)/B_H}$.

When ϵ is not small, the dynamics exhibits relaxation oscillations. On the contrary, when ϵ tends to zero, the concentration variables X and Y show sinusoidal oscillations, and the dynamics are very well approximated by the CGL equation. The correspondence between parameters of the Brusselator and those of the CGL equation has been calculated by several authors [9]–[12] and is given by

$$\beta = \frac{4 - 7A^2 + 4A^4}{3A(2 + A^2)} ,$$
$$\alpha = -A \frac{D_X - D_Y}{D_X + D_Y} . \quad (3)$$

Actually, the spatiotemporal variables $(\mathbf{r}, \tau)$ of Eqs. (2) are related to the independent variables $(\mathbf{x}, t)$ of Eq. (1) by scaling factors in which parameter B is present. In this scaling procedure, the variables t, $\mathbf{x}$, τ and $\mathbf{r}$ are expressed in units (time unit), (space unit), (s), and (cm),

$$(\mathrm{s}) = \epsilon^2 \left(\frac{1 + A^2}{2} \right) (\mathrm{t.u.}),$$
$$(\mathrm{cm}) = \epsilon \sqrt{\frac{1 + A^2}{D_X + D_Y}} (\mathrm{s.u.}). \quad (4)$$

The advantage of studying the CGL equation, whenever it is applicable, is that its treatment is much simpler, numerically as well as analytically. Especially, particular solutions of the CGL equation are known analytically. The simplest nonvanishing solution to Eq. (1) is the homogeneous bulk oscillations defined by $W_0(t) = \exp(-\beta t + \theta_0)$, where θ_0 is a constant. This solution is linearly stable if the Benjamin-Feir condition is satisfied $(1 + \alpha\beta > 0)$. This will be the case in the sequel. Other analytical solutions are a family of plane waves $\{W_q(x,t) = \sqrt{1 - q^2} \exp(-i[\omega t \pm qx]), 0 < q < 1, \omega = \beta + q^2(\alpha - \beta)\}$, which are stable with respect to small perturbations, if the wave number q fulfills the Eckhaus condition [13]

$$q^2 < q_E^2 = \frac{1 + \alpha\beta}{3 + \alpha\beta + 2\beta^2} . \quad (5)$$

Our work is concerned with another spatially inhomogeneous solution of the CGL equation, namely the isolated spiral wave. This solution is described in polar coordinates (r, φ) by the following function:

$$W_s(r, \varphi, t) = F(r) \exp\{-i[\omega t + m\varphi - \psi(r)]\} . \quad (6)$$

Hagan has shown [4] that in an infinite system this type of function may be the solution to the CGL equation, with the boundary conditions: $F(0) = \psi(0) = 0$, $\lim_{r\to\infty} \psi' = q_s$, $\lim_{r\to\infty} F = \sqrt{1 - q_s^2}$, and with q_s as a function of the parameters α and β.

The condition $F(0) = 0$ states that the modulus $|W_s|$ vanishes at the center of the spiral which corresponds to the intersection of the curves $\mathrm{Re}\, W_s = 0$ and $\mathrm{Im}\, W_s = 0$, where Re and Im denote, respectively, the real and the imaginary parts. This point is called a topological defect of the field W_s. The topological charge of the defect is defined as the circulation of the phase gradient of W_s around the defect

$$m = \frac{1}{2\pi} \oint \nabla\theta \cdot d\mathbf{x} . \quad (7)$$

For instance, for a counterclockwise, one-armed spiral, $m = 1$. Then, the conditions as $r \to \infty$ show that W_s is a spiral since, for large values of the coordinate r, the isoconcentration lines obey to the equation $q_s r = \varphi + c$, with c constant. This is the Archimedean spiral with wavelength $\lambda = 2\pi/q_s$. However, when the system is of a finite size we cannot take the limit $r \to \infty$. Nevertheless, by taking an initial condition which has topological charge $+1$ or -1, and imposing zero-flux boundary conditions, we obtain numerical solutions of Eq. (1). These are analogous to isolated one-armed spiral waves if the topological charge $m = \pm 1$ is conserved.

The aim of the present paper is to report some observations on the motion of spiral waves in oscillatory media. This motion may be studied by following the trajectory of the topological defect localized at the center of the spiral. We begin by studying the evolution of a unique defect generated in a two-dimensional square system of length L described by Eq. (1), and subject to the following initial conditions:

$$U(x, y) = \frac{(x - d)}{L} ,$$
$$V(x, y) = \frac{y}{L} . \quad (8)$$

We take the convention that the origin $(0, 0)$ of the coordinate axis coincides with the center of the square. The initial conditions (8) contain a topological defect of charge $m = 1$ at position $(d, 0)$ [see Fig. 1(a)]. In the following the only parameter which will vary is the distance d at which the defect is created.

Let us choose $\alpha = -1$. From Eq. (3) it is seen that this choice corresponds to unequal diffusion coefficients. We shall discuss later what happens when $\alpha = 0$. When α is fixed, and for a given β, the evolution of the system subject to the initial conditions (8) may lead to the formation of a counterclockwise spiral wave, as depicted in Fig. 1(b). The wave number $q_s(\beta)$ of this spiral as shown from the numerical simulations may be evaluated following the prediction of Hagan [4]. On the other hand, we can evaluate the wave number $q_E(\beta)$ corresponding to the Eckhaus condition Eq. (5). Comparing the two functions $q_s(\beta)$ and $q_E(\beta)$ for different values of β, we find that there is a critical value $\beta_c \simeq 0.5$ for which

$$q_s(\beta_c) = q_E(\beta_c) \quad \text{and} \quad \forall \beta > \beta_c : \quad q_s(\beta) > q_E(\beta) .$$

Consequently, taking for example $\beta = 0.6$, the selected wave number q_s does not satisfy the Eckhaus condition (5) and the emitted wave trains are unstable. However, we do observe a stable spiral for $\beta = 0.6$. This paradox was recently highlighted by Aranson *et al.* who pointed out that the Eckhaus instability may be only convective and not absolute [14]. Recall that convective instability means that a perturbation, although amplified, moves away from its initial location and does not necessarily grow locally. This is the case in our simulations. For some initial conditions, a complex transient dynamics is seen around the defect, as a result of the Eckhaus instability. In some case spontaneous spirals may even appear after the breaking of an emitted wave. But after a while, these new defects are pulled toward the boundary where they disappear. As we shall see below, in most cases the only defect which subsists finally is the

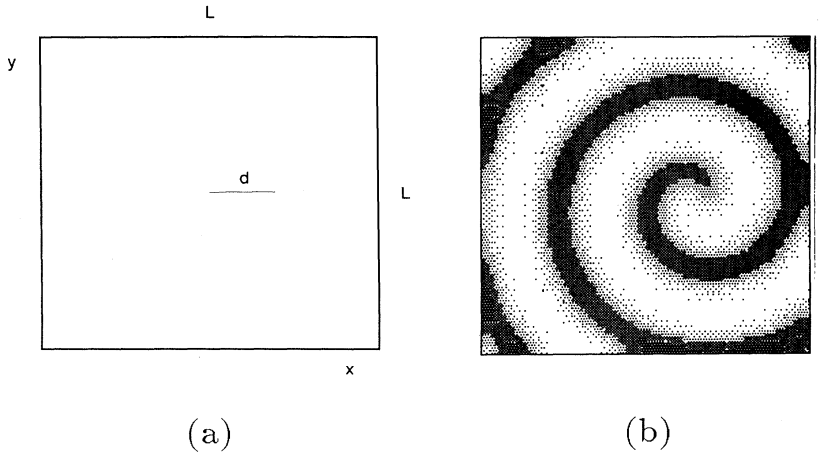

FIG. 1. Counterclockwise spiral wave resulting from the integration of Eq. (1) subject to initial conditions (8) with $d = \frac{3}{8}L$. (a) The initial position of the defect in the square system is situated at distance d from the center of the square. (b) The real part of W is represented by gray shades. Parameters of Eq. (1) are $\alpha = -1$, $\beta = 0.6$ and the system size is $L = 50$.

original one, which was imposed by the initial conditions. As time evolves, the defect usually does not remain motionless, but is pulled by the boundaries on a trajectory circulating along the frontiers of the system.

In the following, we shall choose the parameter $\beta = 0.6 > \beta_c$, as it leads to behaviors which are more interesting than in the case $\beta < \beta_c$. However, we shall discuss in Sec. III what happens in the latter case.

The size of the square, $L = 50$ s.u., is taken such as it corresponds approximately to four times the wavelength of the spiral. With this condition, we may thus consider that the system size is small, compared with the wavelength of the emerging spiral.

In finite systems it is expected that the geometry of the boundaries may influence the self-organizing properties of the system. In Sec. III we show the evolution of the defects, as described above, in two different geometries.

III. SINUSOIDAL OSCILLATIONS

In this section we report numerical experiments on the motion of spiral waves as described previously, in finite systems of square and circular geometries. Both types of geometries are considered in order to investigate which properties are generic for systems of limited size and which effects are due to the particular shape of the boundaries. The dynamics are described by the CGL equation. Thus, we can think of our experiments as the study of chemical spiral waves in an oscillating medium near a Hopf bifurcation.

A. Square geometry

In our numerical experiments, Eq. (1) is solved by means of a finite-difference method (cf. the Appendix), with initial conditions given by expression (8). At each time step, the new position of the defect is monitored by computing the absolute minimum of $|W| \approx 0$, in a region close to the preceeding position.

Our results are summarized in Fig. 2. As the distance d of the initial position of the defect is varied continuously from 0 to $L/2$, five different cases must be distinguished for the evolution of the system.

(i) $0 \leq d \leq \frac{2}{40}L$. The defect is attracted to a fixed position situated at the center of the system.

(ii) $\frac{2}{40}L < d \leq \frac{7}{40}L$. The defect follows a trajectory along a square of length $L/4$ [Fig. 2(a)]. The motion has a mean velocity equal to 5.7 10^{-3} s.u./t.u. This motion

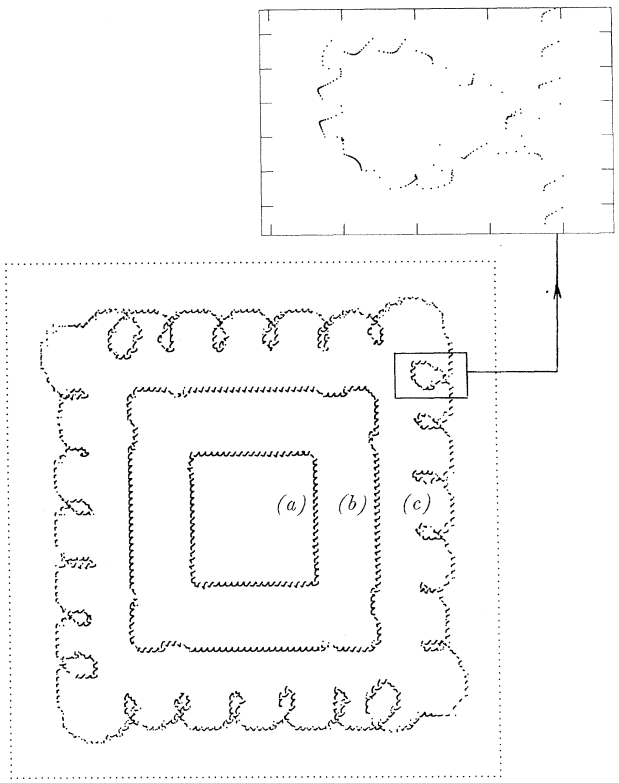

FIG. 2. Multiple asymptotic trajectories followed by the defect in the square system for different values of d. (a), (b), and (c) correspond, respectively, to cases (ii)–(iv). Parameters of Eq. (1) are the same as in Fig. 1. The system is covered by 80 × 80 boxes. The rectangle in the top-right corner is a magnification of a loop.

is very slow as compared with the phase velocity of the emitted waves which is 0.57 s.u./t.u.

(iii) $\frac{7}{40}L < d \leq \frac{12}{40}L$. The defect is attracted to another closed trajectory. The latter is of the form of a square of length $L/2$ [Fig. 2(b)]. However, some distortions are seen due to corner effects. This motion is a little faster than in the preceeding case as the revolution of the defect along this trajectory has a velocity of 8.7 10^{-3} s.u./t.u.

(iv) $\frac{12}{40}L < d \leq \frac{16}{40}L$. In this case, although the defect again follows the boundaries of the system, the trajectory shows almost regular loops with some distortions at the corners, as depicted on Fig. 2(c). This trajectory, composed mainly of a translational and a rotational motion, is closed and attracting. The mean velocity of the evolution is 0.49 s.u/t.u., which is much faster than the above-cited cases. There is a modulation of the wavelength of the emitted spiral.

(v) $\frac{16}{40} < d \leq \frac{20}{40}L$. The defect is attracted by the boundaries and vanishes there.

In all cases, the revolution of the defect around the frontiers of the system is counterclockwise. We verified that with an initial condition of opposite topological charge, i.e., $m = -1$, the motion is clockwise.

It must be noted that all these closed trajectories are due to boundary effects. Therefore they are not of the same nature as the motion of the core of a spiral seen in excitable media [15] or in oscillatory media [16]. In an infinite medium, this latter motion would persist, whereas the motion we report here would not be present.

In our numerical simulations, the two-dimensional system is divided in 80 × 80 boxes which may be identified with a network of coupled oscillatory elements. The discrete character of the system is reflected by the tiny oscillations which are superimposed to the main trajectories and which show a wavelength of $L/80$, i.e., the length of a box. Figure 2 shows a magnified view of a part of a loop. These results show that the dynamics of discretized systems, as compared with the continuum limit, is much more complex.

The three closed trajectories (ii)–(iv) can be considered as global-limit cycles of the system. Indeed, they represent time-periodic solutions of the equations, which are stable with respect to small perturbations. The basins of attraction of these limit cycles are probably separated by four other trajectories between the different attractors, which correspond to periodic repellors of the dynamics. These repellors manifest themselves for values of d corresponding to the bounds of intervals given in (ii)–(iv). Indeed, for these values the dynamics show long transients, which reveal the presence of the stable manifolds associated with the repellors. In some cases these transients are accompanied by the creation of defects which disappear later. These chaotic transient regimes may be attributed to the convective instability of the emitted waves, as mentioned in the Sec. II. In all cases the topological charge $m = 1$ is asymptotically conserved, except in case (v) where m is decreased from 1 to 0 because of the extinction of the spiral.

The looping motion reported in case (iv) is related to the Eckhaus instability. Indeed, as mentioned in Sec. II, the value of β has been chosen so that the selected wave number $q_s(\beta)$ of the spiral does not satisfy the Eckhaus condition (5). On the other hand, we have performed other numerical simulations with $\beta < \beta_c$, i.e., in the case where there is no Eckhaus instability. In this situation, no looping motion is observed.

Moreover, we observe also that if β is close to β_c, $0 < \beta - \beta_c \ll 1$, oscillations of small amplitude appear in the trajectory of the spiral core moving along the boundaries. These oscillations are amplified for greater value of β and give rise to the looping motion described in (iv). Therefore we conclude that the looping motion indicates the presence of the Eckhaus instability which occurs for $\beta > \beta_c$.

B. Circular geometry

In Sec. III A we saw trajectories of the defect generating a simple spiral wave in a square geometry. We saw the multiplicity of asymptotic states of the system as a function of the initial conditions, and in particular the existence of a looping trajectory near the boundaries of the square.

Our aim in this section is to investigate whether these properties are the results of square geometry and, more specifically, corner effects, or are they intrinsic to the system considered. In order to avoid corner effects, a circular geometry will be considered.

First, we perform the same experiments as above in a disk circumscribed to the square, i.e., of radius $R = \frac{\sqrt{2}}{2}L$. Details on the numerical method are briefly given in the Appendix.

A spiral wave is initiated with the initial conditions given by Eq. (8) in which d plays the role of a control parameter. When the distance d is increased from 0 to its maximal value R, only three asymptotic states are possible in the present case.

(i) $0 \leq d < \frac{2}{3}R$. The defect is attracted to a circular trajectory. This situation is quite comparable to the case (iii) of the square. In both cases, the trajectory lies at the same constant distance from the border. The mean speed of this motion (23 10^{-3} s.u./t.u.) is faster than in the square (8.7 10^{-3} s.u./t.u.). Figure 3 shows such a spiral in the disk.

(ii) $\frac{2}{3}R \leq d < \frac{50}{57}R$. As in the case of the square geometry the trajectory with almost regular loops again follows the boundaries. The mean velocity of this motion as well as the mean distance of the defect from the boundaries are the same as in the preceeding values measured in the square. Moreover, the wavelength of the short loops is also of the same order for the circle and the square system.

(iii) $\frac{50}{57}R \leq d \leq R$. The defect is attracted by the boundary, the spiral disappears, and the system returns to the bulk oscillations.

We should mention that in case (ii) the dynamics may be a bit more complicated than the corresponding situation in the square. In fact, for some values of d, there is an intermittent breaking of the wave train emitted by the spiral, concomittant with the onset of another defect at the same distance from the border as the center of the

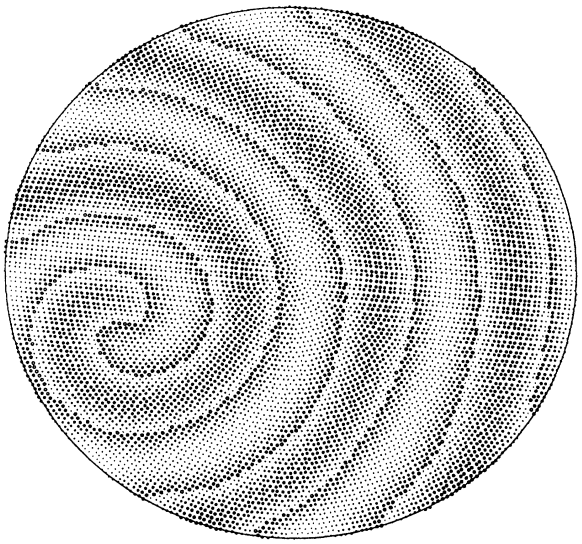

FIG. 3. A spiral wave in a disk of radius $R = \sqrt{2}L/2$. The defect was initially situated at the center of the disk and has moved to follow a counterclockwise circular trajectory of radius $\frac{2}{3}R$. Parameters of Eq. (1) are the same as in Fig. 1.

spiral. This new defect travels on a circular trajectory, without loops.

We also performed the same simulation in a disk inscribed in the square, i.e., of radius $R = L/2$. Surprisingly, in this circular domain, we lose the multiplicity of asymptotic trajectories as a function of the parameter d for the initial conditions (8). In fact, there is only one stable trajectory which attracts the initial defect along the boundary. Figure 4 shows the movement of a defect

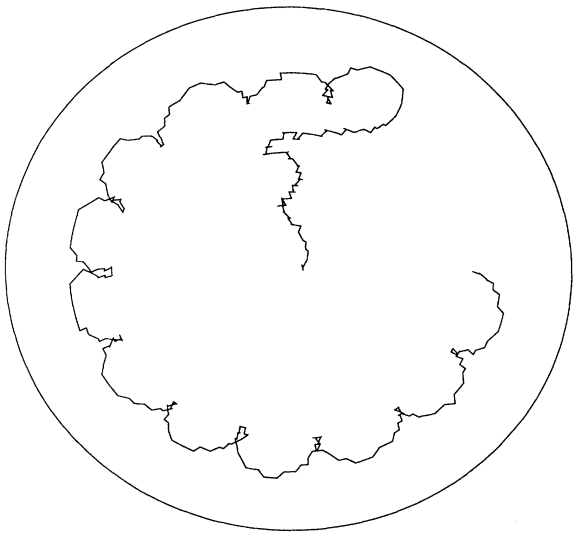

FIG. 4. Looping motion of a defect situated initially at the center of the disk of radius $R = L/2$. The initial conditions (8) were initiated at $d = 0$. Small irregularities of the trajectory are due to discretization effects.

situated initially at the center of the disk. After a few rotations, the defect starts to get closer to the circular frontier and follows a counterclockwise trajectory.

The results reported in this section were obtained close to a Hopf-bifurcation point. It is interesting to see the behavior of spiral waves in a medium undergoing relaxation oscillations.

IV. RELAXATION OSCILLATIONS

The experiments presented in Sec. III describes the dynamics of spiral waves arising in the Brusselator model with $A = 1.631$, $D_X/D_Y = 4.17$, and $B = (1+\epsilon^2)\,3.66$. For ϵ sufficiently small, thus close to the Hopf bifurcation, we expect to find quantitative agreement between the solutions of the CGL equation and the direct integration of Eqs. (2) in a system of length $\mathcal{L}$. With the value of $D_Y = 10^{-5}$ cm^2/s, and due to the scaling factors (4), the size of the Brusselator system correponding to Sec. III is $\mathcal{L} = 3.8\ 10^{-3}/\epsilon$ cm.

As ϵ is increased, the CGL description is no more valid because the oscillations lose their sinusoidal shape and exhibit relaxation oscillations, characterized by a short episode of rapid variation followed by a longer time interval of slow variation. This feature is reflected by the onset of sharp fronts of concentration and trigger waves. The system is expected to behave more like an excitable medium.

With relaxation oscillations, it becomes more difficult to initiate an isolated spiral wave. For example, the initial conditions given by Eqs. (8) do not lead anymore to a sustained spiral. In order to favor the birth of a spiral wave, special initial distribution of the concentration variables must be mapped in the space around the defect. Following the idea of Erneux and Kaufman we use the initial conditions which creates a spiral wave around the position $(0, d)$ [9],

$$\begin{pmatrix} X(r_1, r_2) \\ Y(r_1, r_2) \end{pmatrix} = \begin{pmatrix} A \\ B/A \end{pmatrix} + c \begin{pmatrix} \chi(\sigma) - A \\ \xi(\sigma) - B/A \end{pmatrix} J_1(k_1 \rho/\Lambda)\ . \tag{9}$$

In this expression, $r_1 = \rho\cos(\sigma)$, $r_2 - d = \rho\sin(\sigma)$, $\chi(\sigma) = X_0(\sigma T/2\pi)$, and $\xi(\sigma) = Y_0(\sigma T/2\pi)$, where $(X_0(t), Y_0(t))$ is the homogeneous limit cycle solution of the Brusselator of period T. Λ is the supremum of distances from the $(0, d)$ position to another point in the system, c is an arbitrary constant, and k_1 is the first zero of the derivative of the Bessel function J_1.

Now, we consider the Brusselator model with the same parameters as above, but with the value of $\epsilon = 1$ in order to get relaxation oscillations. Both square and circular geometries will be examined.

We first consider a square system of length $\mathcal{L} = 3.8 \times 10^{-3}$ cm. An isolated spiral wave is created by the initial conditions (9). Here again the system can settle on several asymptotic states, depending on the initial position of the defect. For $d = 0$, as in the case of small ϵ, the spiral rotates steadily at the center of the square with a period of $T = 3.67$ s (Fig. 5). Note that here the

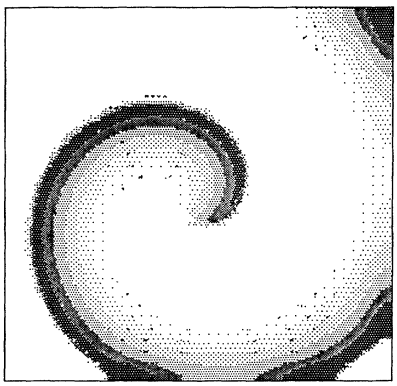

FIG. 5. Isolated spiral wave appearing in the evolution of the Brusselator equations (2) subject to the initial conditions (9) at $d = 0$. The concentration variable X is represented by gray shades. The zero-flux boundary conditions force the isoconcentration lines to be perpendicular to the boundaries. Parameters $A = 1.631$ and $B = 7.32$ are such that the dynamics present relaxation oscillations. The other parameters of Eqs. (2) are $D_X = 4.17 \times 10^{-5}\text{cm}^2/\text{s}$, $D_Y = 10^{-5}\text{cm}^2/\text{s}$, and the system size is $\mathcal{L} = 3.8 \times 10^{-3}$ cm.

wavelength of the spiral is roughly $\mathcal{L}/2$. As d is increased, similar asymptotic states are observed. For $d = \mathcal{L}/8$, the spiral seems to rotate around a fixed position. This situation was observed for more than 1000 rotations of the spiral. For $d = 2/8\,\mathcal{L}$, the defect of the spiral is attracted to a square trajectory of length $3/8\,\mathcal{L}$ on which the spiral drifts very slowly with a velocity of 0.29×10^{-6} cm/s. Finally, for $d = 3/8\,\mathcal{L}$, the spiral is attracted to another square trajectory of length $2/3\,\mathcal{L}$. The latter is no more of the looping type, but reduces to a simple translation along the boundaries. The velocity of the slow drift of the spiral is 1.2×10^{-5} cm/s. Thus the relaxation oscillations simplifies the motion of the spiral.

Later on, the size of the square was increased to $2\,\mathcal{L}$. Here also the closest trajectory to the boundaries, which lies at the same distance from it than in the square of length $\mathcal{L}$, is only a translational motion.

Next we perform the numerical experiment with the Brusselator in a disk inscribed to the square, i.e., of diameter $\mathcal{L}$. As in the sinusoidal case, there is no multistability of trajectories, and in particular the central position of the circle is an unstable position for the defect. There is only one stable trajectory along the circular boundaries, but contrary to the sinusoidal oscillations, there is only a translational motion and no looping motion is seen.

In conclusion, we see that relaxation oscillations give rise to similar behaviors as for the CGL equation in small systems. Looping motions are not present with relaxation dynamics. However, with relaxation oscillations we can expect intrinsic motions of the spiral core, such as the meandering in excitable media. This fact was effectively observed by Wu, Chee, and Kapral [16].

V. DEFECT IN THE PRESENCE OF OBSTACLES

Let us consider again a two-dimensional oscillatory medium, so that the CGL description remains valid. However, presently an impermeable barrier divides the square in two compartments. The two compartments communicate through an opening of length l [17].

We start our numerical simulations in the same manner as above. The value of d is fixed to $L/8$.

When the size of the opening l is decreased from its maximal value $l = L$, several behaviors are observed. Figure 6(a) shows a typical trajectory of the defect when the opening is sufficiently large ($l = L/2$). The defect visits the two compartments, following a complex closed curve. We observe that during the passage through the aperture, the motion is much slower than in the other parts of the system.

When the opening size is reduced, the defect does not travel in the entire system. It is constrained to a closed path in one compartment, as illustrated in Fig. 6(b) ($l = L/5$). In the second compartment no defects are observed, but irregular target waves like activity are emitted from the opening (not shown).

In addition to these typical behaviors, for particular values of l, other phenomena may appear. For example, for $l = 3/4\ L$, the initial defect starts in one compartment, passes through the opening into the second compartment, and then is attracted to a small closed circuit a short distance from the opening [see Fig. 6(c)]. Another type of behavior is also obtained for $l = L/10$. In this case, as the original defect describes a trajectory in the first compartment, a second defect is created in the next compartment. After a short period of coexistence, the original defect disappears and the new one is stabilized in a fixed position in the second compartment.

VI. DISCUSSION AND CONCLUSION

In this paper, with the help of numerical simulations, we studied the motion of an isolated spiral wave in finite oscillating media.

We showed that when the spiral center, the topological defect, is created near the boundaries, it moves along the boundary, independent of the geometry of the system. This drift may be observed with sinusoidal as well as relaxation oscillations. The speed of the spiral motion substantially slows down when the trajectory takes place far from the boundary.

The origin of this motion is probably due to the breaking of translational symmetry of the equations describing the dynamics, resulting from the presence of boundaries. In fact, the zero-flux boundary conditions create a mirror image of the isolated spiral beyond the boundary. This image plays the role of a virtual spiral which interacts with the real one in a similar way as in a pair of spirals. Therefore, the motions reported here could be compared, in first approximation, to the motion of a pair of spirals, which was studied recently analytically [16, 18, 19] as well as numerically [16, 20, 21]. These studies show the rapid decreasing of the interaction of a pair of spirals as the distance between their cores is increased. The possibility

of the drift of the pair in a direction perpendicular to the line joining the centers of the spiral is also discussed. Sakaguchi [20] points out that this motion, which is a translation, is a nonvariational effect, and thus it would not be present in the real Ginzburg-Landau equation.

Another generic feature of spiral waves in bounded oscillating media is that the asymptotic dynamics can take the form of closed trajectories which are attracting and are followed in a strictly periodic manner. Such asymptotic states constitute global-limit cycles of the system. In a sufficiently large system, multiplicity of asymptotic trajectories may be observed. This multistability is reduced in a circular geometry as compared with the square geometry. In particular, in our experiments the center of the square is a stable position for the center of the spiral, whereas in the disk, it is an unstable position. When the system size is reduced, this central position may become stable also in a disk [22]. When the system size is further reduced, there is a critical value below which no stable spiral wave is observed [9].

In the case of sinusoidal oscillations, we could observe an interesting looping motion of the spiral core along the boundaries, composed of a translational and a rotational motion. During this motion the wavelength of the spiral wave is modulated. This modulation may be attributed to the Eckhaus instability, as discussed in Sec. III. In the case of relaxation dynamics, no such looping motions were observed. However, in this case the intrinsic motion of the defect may be observed [16].

In this paper we discussed a system with unequal diffusion coefficients. We have also performed numerical experiments with equal diffusion coefficients, i.e., $\alpha = 0$

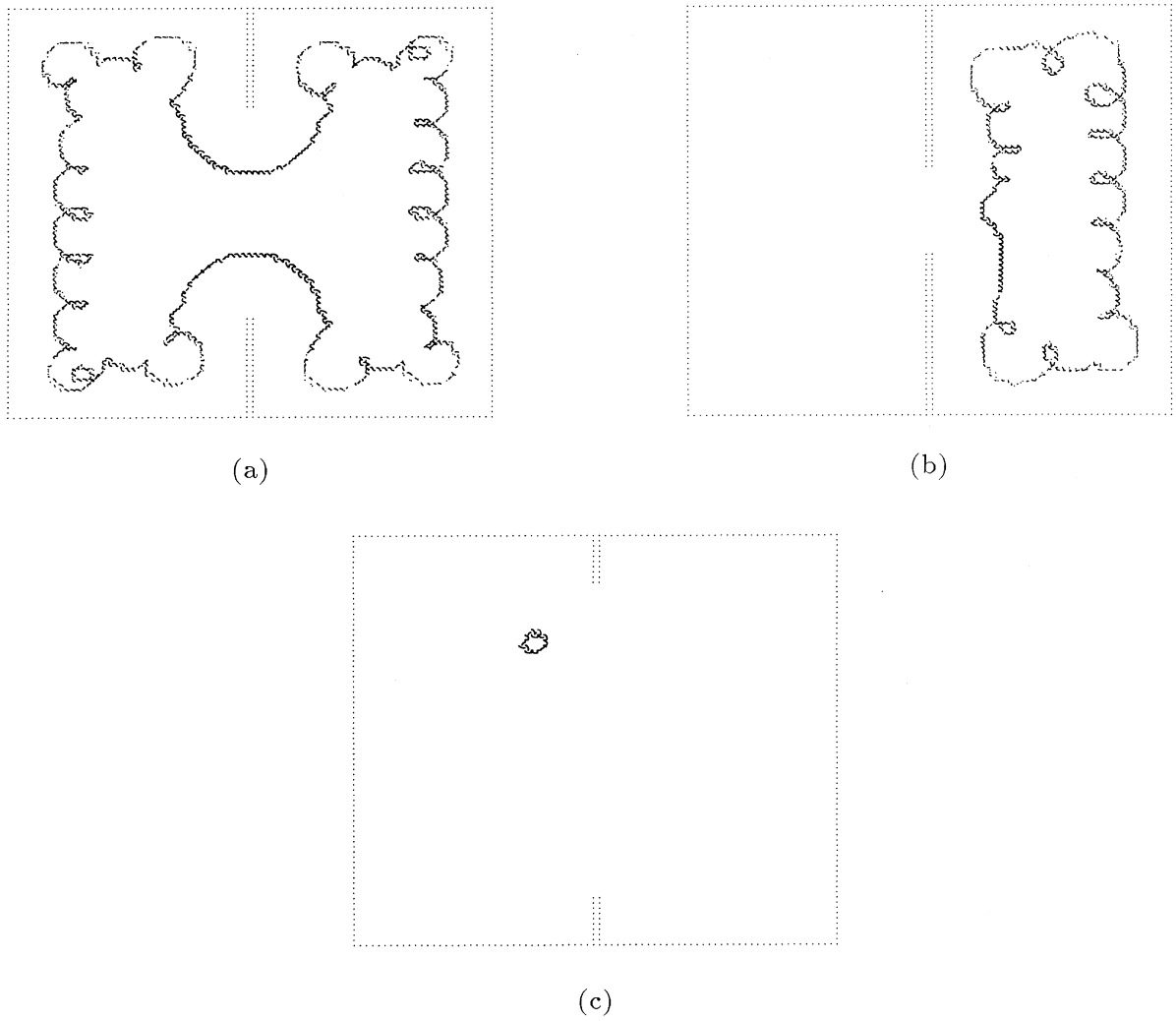

FIG. 6. A square system is partitioned into two compartments by an impermeable barrier. An opening of size l allows the propagation of waves between both compartments. Evolution of the initial conditions (8), with $d = \frac{3}{8}L$, creates a spiral wave, whose center circulates on a closed trajectory. (a) For $l = L/2$, the trajectory passes in both compartments periodically. (b) For $l = L/5$, the trajectory is trapped in one compartment. (c) For $l = \frac{3}{4}L$, the defect initially in the right compartment passes through the opening and is attracted to a small closed trajectory in the left compartment. The parameters of Eq. (1) are the same as in Fig. 1.

in the CGL equation. We have chosen a value of $\beta = 1.5$ such that the same wavelength as considered in this paper is selected, and we observed the same qualitative phenomena. However, in this case no looping motion was observed, although the selected wave number q_s was in the range of Eckhaus instability. Thus it seems that the looping motion involves $\alpha \neq 0$, which corresponds to unequal diffusion coefficients for reaction-diffusion systems.

The main results reported in this paper describe the behavior of an *oscillating* reaction-diffusion system close to a supercritical Hopf bifurcation. In this regime, the dynamics may be described by the complex Ginzburg-Landau equation, which is a *normal form*, i.e., a universal equation which is independent of the specific kinetics of chemical reactions or any specific model. Therefore our results are quite general, and are not limited to the Brusselator model. Moreover, they apply to real systems like the BZ reaction, placed in appropriate conditions or any real or model chemical oscillatory reaction of the same type. Our numerical studies predict a variety of phenomena which could be experimentally verified in an oscillating chemical reaction-diffusion system of small size.

ACKNOWLEDGMENTS

This work was supported by the SPPS (Service de Programmation de la Politique Scientifique) of the Belgian Government in the context of the IMPULSE project and by the EEC (ESPRIT, Basic Research, Project No. 3234). We thank P. Borckmans for interesting comments.

APPENDIX: NUMERICAL METHODS

Numerical integration of Eq. (1) and Eqs. (2) is carried out with finite-difference methods. The square vessel is divided in a grid of $N \times N$ nodes on which the Laplacian operator ∇^2 as well as the zero-flux boundary conditions are approximated by the well-known five-node formula [23]. By this procedure, the partial-differential equations are reduced to a large system of coupled ordinary differential equations which are solved with the following methods.

Equation (1) is integrated with the Merson method which is based on a four-order Runge-Kutta algorithm. This method is endowed with a control of integration step such as to achieve a given precision [24]. Most of the computations are performed with $N = 80$ and a relative accuracy of 10^{-3}. Numerical calculations were also performed with $N = 160$ and an accuracy of 10^{-5}. No significant change on the quantitative behavior was observed.

The simulations of Eqs. (2) are performed with the simple Euler method. Here we considered $N = 160$ and a time step $\delta t \sim 10^{-2} - 10^{-3}$.

In the circular domain, Eq. (1) and Eqs. (2) are integrated, using a particular grid generation, suggested by Zykov [25]. The grid generation is based on polar coordinates with a variable angular distribution of nodes as a function of the radius.

The idea of the method is the following. The disk of radius R is divided in N concentric circles, equally spaced by a distance of $\delta r = \frac{R}{N}$. On each circle of radius $K\delta r$, $(1 \leq K \leq N)$, $6K$ nodes are equally distributed. In addition, a node is placed at the center of the disk. This procedure covers the disk with $3R(R+1)+1$ nodes, forming a grid of almost constant density. The coefficients of the discretized Laplacian operator are obtained by linear interpolation of the neighboring nodes.

The grid generated by this procedure possesses a hexagonal symmetry, i.e., only rotations which are a multiple of $\frac{\pi}{3}$ leave the grid invariant. In some numerical simulations, this symmetry is reflected in the solution of Eq. (1) and Eqs. (2). These spurious effects may be eliminated by imposing a random rotation of the grid during the integration of the equations.

Note that a circular domain may also be discretized inside a square grid. In this case, the finite-difference approximation of the Laplacian is simpler, but special care must be taken in satisfying the boundary conditions. The advantage of a polar grid is that the boundary conditions are satisfied very simply. Moreover, the fact that we observed the same phenomena with different discretization methods shows that our observations are really related to continuous media subject to reaction and diffusion processes.

---

* Electronic address: jasepulc@ulb.ac.be

[1] J.M. Davidenko, A.V. Pertsov, R. Salomonsz, W. Baxter and J. Jalife, Nature **355**, 349 (1992).
[2] J. Lechleiter, S. Girard, E. Peralta, and D. Clapham, Science **252**, 123 (1991).
[3] A.C. Newell, in *Lectures in Applied Mathematics* (American Mathematical Society, Providence, 1974), Vol. 15.
[4] P.S. Hagan, SIAM J. Appl. Math. **42**, 762 (1982).
[5] S.Y. Cai and A. Bhattacharjee, Phys. Rev. A **43**, 6934 (1991).
[6] P.S. Hagan and M.S. Cohen, Theor. Biol. **93**, 881 (1981).
[7] I. Prigogine and R. Lefever, J. Chem. Phys. **48**, 1695 (1968).
[8] G. Nicolis and I. Prigogine, *Self-Organisation in Non-equilibrium Systems* (Wiley, New York, 1977).
[9] Th. Erneux and M. Herschkowitz-Kaufman, Bull. Math. Biol. **41**, 767 (1979).
[10] D. Walgraef, G. Dewel, and P. Borckmans, J. Chem. Phys. **78**, 3043 (1983).
[11] P.H. Richter, I. Procaccia, and J. Ross, in *Advances in Chemical Physics*, edited by I. Prigogine and Stuart A. Rice (Wiley, New York, 1980), Vol. 43, p. 235.
[12] Y. Kuramoto, *Chemical Oscillations, Waves, and Turbulence* (Springer-Verlag, Berlin, 1984).
[13] J.T. Stuart, F.R.S. DiPrima, and R.C. DiPrima, Proc. R. Soc. London Ser. A, **362**, 27 (1978).
[14] I.S. Aranson, L. Aranson, L. Kramer, and A. Weber, Phys. Rev. A **46**, R2992 (1992).
[15] A. Winfree, Chaos **1**, 303 (1991).
[16] X.-G. Wu, M.-N. Chee, and R. Kapral, Chaos **1**, 421 (1991).
[17] J.A. Sepulchre and A. Babloyantz, Phys. Rev. Lett. **66**,

1314 (1991).
[18] I.S. Aranson, L. Kramer, and A. Weber, Physica D **53**, 376 (1991).
[19] L.M. Pismen and A.A. Nepomnyashchy, Phys. Rev. A **44**, 2243 (1991).
[20] H. Sakaguchi, Prog. Theor. Phys. **82**, 7 (1989).
[21] E. Bodenschatz, A. Weber, and L. Kramer, in *Nonlinear Wave Processes in Excitable Media*, Vol. 244 of *NATO Advanced Study Institute Series B: Physics*, edited by A. V. Holden, M. Markus, and H. G. Othmer (Plenum, New York, 1989).
[22] Th. Erneux and M. Herschkowitz-Kaufman, J. Chem. Phys. **66**, 248 (1977).
[23] W.H. Press, B.P. Flannery, S.A. Teukolsky, and W.T. Vetterling, *Numerical Recipes. The Art of Scientific Computing* (Cambridge University Press, Cambridge, 1986).
[24] M. Kubicek and M. Marek, *Computational Methods in Bifurcation Theory and Dissipative Structures* (Springer-Verlag, New York, 1983).
[25] V.S. Zykov (private communication).